275859 High Resolution Airborne FMCW Radar Reveals the Well-Known Puzzle of Warm Rain Formation in a Small Cumulus

Ming Fang and Bruce Albrecht
Rosenstiel School of Marine and Atmospheric Science, University of Miami

1. Introduction

Warm rain is defined as the rain originating from clouds with their tops under freezing level. It contributes 31% to the total rain amount and 72% to the total rain area in the tropics (Lau and Wu, 2003). It plays a very important role in water and energy cycle of the climate system. The mechanisms responsible for the formation of rain in warm clouds have been debated for over six decades (Small and Chuang, 2008). The central question is how it forms as rapidly as it is sometimes observed. It has been realized for decades that turbulence may play a significant role in warm rain formation. There are many publications about this topic, such as Saffman and Turner (1956), Riemer and Wexler (2005), Falkovich, et al. (2006), Xue, et al. (2008) among others. However, the majority of the publications are theoretical or numerical simulation studies, and observations in the real world are limited. One reason for this might be that warm rain often occurs over the ocean, which makes observation difficult; another reason for this might be that the vertical air velocity is not easy to measure although it closely relates to dynamics and microphysics in clouds. Aircraft penetrations in clouds and precipitation can offer direct (in-situ) measurement of the vertical air motion. However, these measurements are limited to 1-D (flight level) and aircraft penetration to areas of strong turbulence is limited for safety reasons. Using Doppler radars to measure vertical air motion in precipitating clouds has been exploited more than five decades (Probert-Jones and Harper 1961; Doviak and Zrnic 1993). Ground-based vertically pointed Doppler radars can provide a 2-D time-height

velocity field, but they can only observe the cloud or precipitation passing over the radar site. Airborne Doppler radars combine the advantages of aircraft mobility and the radar 2-D measurements and make it possible for investigators to study meteorological phenomena in remote region or over the ocean and allow investigators to select features of interest and obtain more comprehensive characterizations of the clouds and precipitation structures (Heymsfield et al. 1996; French et al. 1999). In 1980s, Bragg scattering (Wakasugi et al. 1986; Gossard 1988; Rogers et al. 1993; May and Rajopadhyaya 1996; Rajopadhyaya et al. 1998) observed by wind profilers (Doppler radars operating at VHF and UHF) were used to extract the vertical air motion. However, the antenna size of a wind profiler is too big to be deployed from a scientific research aircraft. Over the past decade, the vertical air motion in precipitation has been retrieved using short wavelength (e.g., λ=3.2 mm, 95-GHz frequency) cloud radars (Kollias et al. 2002; Kollias et al. 2003; Kollias et al. 2007; Giangrande et al. 2010) by using Mie scattering signatures in Doppler spectra as first proposed by Lhermitte (1988). Compared to wind profilers, 95-GHz Doppler radars are compact, highly portable and available on moving platforms (e.g., Li et al. 2004). However, the platform motion can shift Doppler spectra and Mie maxima and minima. This study will use Doppler spectra observed by an airborne FMCW Doppler radar. After motion contaminations are removed, the first Mie minima in airborne Doppler radar spectra are used to retrieve vertical air velocities that are in turn used to investigate the turbulence characteristics in the small cumulus clouds.

2. 95-GHz FMCW Doppler radar and data

To observe cloud-aerosol interactions, associated with precipitating and non-precipitating cumuli over the tropical ocean,

the Key West Aerosol Cloud Experiment (KWACEX) was performed in May 2012. The Collaborative Institute for Remotely-Piloted Aircraft Studies (CIRPAS) research aircraft Twin Otter (TO) was the principal observing platform. Twin Otter was equipped with aerosol-, cloud-, and precipitation-probes, and standard meteorological instruments for observing the mean and turbulent thermodynamic and wind structure.

A solid-state Frequency Modulated Continuous Wave (FMCW) 95 GHz Doppler radar (Mead et al. 2003) was mounted on the top of the aircraft in an upward facing mode and normal to fuselage. It has a 10 m range resolution, 0.7 degree angular resolution and about 0.25 s time resolution. The radar parameters are listed in table 1.

TABLE 1. Characteristics of a FMCW radar.

Parameter	**Value**
Center frequency (GHz)	94.2
Peak transmit power (dBm)	30
Transmit duty cycle (%)	6.25
PRF (Hz)	63.145
Chirp pulse bandwidth (MHz)	Variable; up to 20
Maximum range (m)	3962.5
Maximum velocity (m s^{-1})	12
Range Resolution (m)	10
Receiver noise figure (dB)	7.0
Antenna Diameter (cm)	30 (12 inches)
Antenna Gain (dB)	46
Antenna Beam width (degrees)	0.7
FFT Number	64
Radar beam orientation	Up-looking (perpendicular to the aircraft centerline)

3. Aircraft motion correction and uncertainties

The FMCW radar is mounted on the top of the aircraft in an upward vertically pointing beam mode. The radar beam is usually perpendicular to the aircraft centerline, and sometimes is tilted a few degrees off zenith forward to offset the mean pitch angle. Therefore, the observed vertical component of the Doppler velocity is contaminated by the aircraft motion. To retrieve vertical air velocity, the motion of Twin Otter aircraft has to be removed. The Twin Otter is equipped with a variety of instruments to measure various meteorological and cloud microphysical parameters. The position, attitude angles and velocity of the TO were determined using the global positioning system (GPS) technique with relatively higher accuracy (Kalogiro and Wang, 2001). The accuracy of position, attitude angles and velocity are 5 m, 0.1^{o} and 0.05 ms^{-1} respectively. Heymsfield (1989) derived a set of equations for nadir or zenith viewing radars that can be used to remove the platform motion and transform the velocity from platform-relative coordinate system to earth-relative coordinate system. In this study, considering radar beam might be titled a few degrees forward sometimes as aforementioned, we use the more general results proposed by Lee et al. in 1994 (L1994 hereafter) that can be applied to a beam pointed in any direction. In fact, in addition to aircraft motion, there are other contaminators but aircraft motion is the largest and most significant one. Formulas used to remove contaminations are described in Appendix A. Different from those in Eq. 26 of L1994, on the left side of Eq. A4a, $\overline{w}$ and $\bar{v}_t$ have replaced w and v_t. It is well known that radar measured velocity is not a point velocity, but a volumetric mean velocity weighted by reflectivity and radar beam pattern; over bars indicate this volumetric average and emphasize that, only

under some conditions, the radar measured air velocity can be interpreted as an air velocity at a point. From spectral point of view, the left side of Eq. A4a is the mean of a spectrum due to both vertical air motion and terminal velocity associated with particle size distribution (PSD) (Fang et al. 2012; Fang and Doviak 2007). The spectrum of vertical air motion convolves with the spectrum of terminal velocity. It is difficult to separate two spectra from each other. However, Mie technique does not require two spectra to be separated. To simplify the problem, this study assumes that the vertical air velocity and PSD are uniform in radar resolution volume; uniform PSD is equivalent to a uniform reflectivity. With these assumptions, the over bars in Eq. A4a can be removed and the Doppler spectrum can then be completely attributed to the particle size distribution but shifted by a *w*. In this case, the retrieved *w* is equivalent to the vertical air velocity at a point.

On the right hand side of Eq. A4a, V_r is directly measured by the radar and all other terms, except I_1, can be determined from GPS measured aircraft attitude angles and velocities. I_1, or Eq. A4b represents a contribution from horizontal wind. To estimate I_1, a seventh order polynomial fitting is made to soundings of horizontal wind speed and direction that were obtained between 19:24:00 and 19:39:00 UTC on 22 May 2012 when aircraft climbs from 20 m to 2.5 km above sea surface. After the determination of aircraft height, the fitted profiles of wind speed and direction are then used to calculate I_1 at each radar range gate. Fig. 1 shows three time series of correction terms at 100 m above radar level (ARL). The black curve represents term $WG + I_2/\sin\phi$, due to aircraft motion (including both horizontal and vertical motion); the red curve represents term $I_1/\sin\phi$, due to horizontal wind and blue curve represents term $\left(I_3 + I_4\right)/\sin\phi$, due to apparent

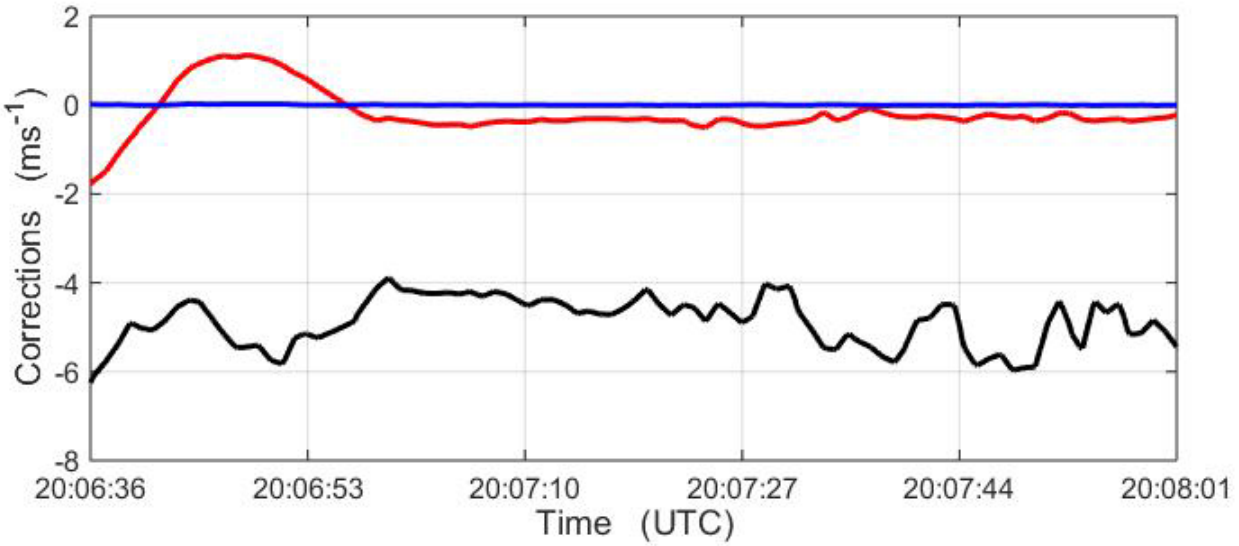

Fig. 1. Correction terms related to aircraft motion (black), horizontal wind (red) and apparent velocity (blue).

velocity. It can be seen that both aircraft motion and horizontal wind terms are significant; aircraft motion is the largest contributor and the contribution from apparent velocity is negligible. After all terms on the right hand side of Eq. A4a are calculated at each radar range gate, one obtains a motion contamination-removed Doppler spectrum that can be used to generate Doppler moments. An example of the zeroth-moment (radar reflectivity) and the first-moment (Doppler velocity) of the 95-GHz FMCW Doppler spectrum from a relatively shallow cumulus clouds are shown in Fig. 2. The aircraft observations were made near the cloud base at an air speed of about 60 ms^{-1} and an altitude of 450 m above sea level. The aircraft within this 6 km long racetrack intercepted the shallow convective clouds observed between 20:06:20-20:08:00. The average cloud top height is about 1.7 km. There might be three cells with their centers around 20:06:50, 20:07:20 and 20:07:40 UTC respectively. The upper portion of the second cell is tilted with height and rides over the first cell. Despite their shallow nature, these clouds produce strong radar reflectivity (e.g., maximum reflectivity of -8.5 dBz) due

to the presence of large precipitating size particles that are located around the dark red regions in Fig. 2a. Particles exceeding 1.69 mm in sizes will be able to generate the Mie resonance in the Doppler spectra. Both Fig. 2b and 2c show Doppler velocity, but the aircraft motion and horizontal wind contamination have been removed in Fig. 2b whereas in Fig. 2c, they have not. Comparing to Fig. 2c, the predominant upward motion in clouds has been replaced by downward motion after contaminations have been removed in Fig. 2b. The downward motion is mostly associated with the precipitation shaft

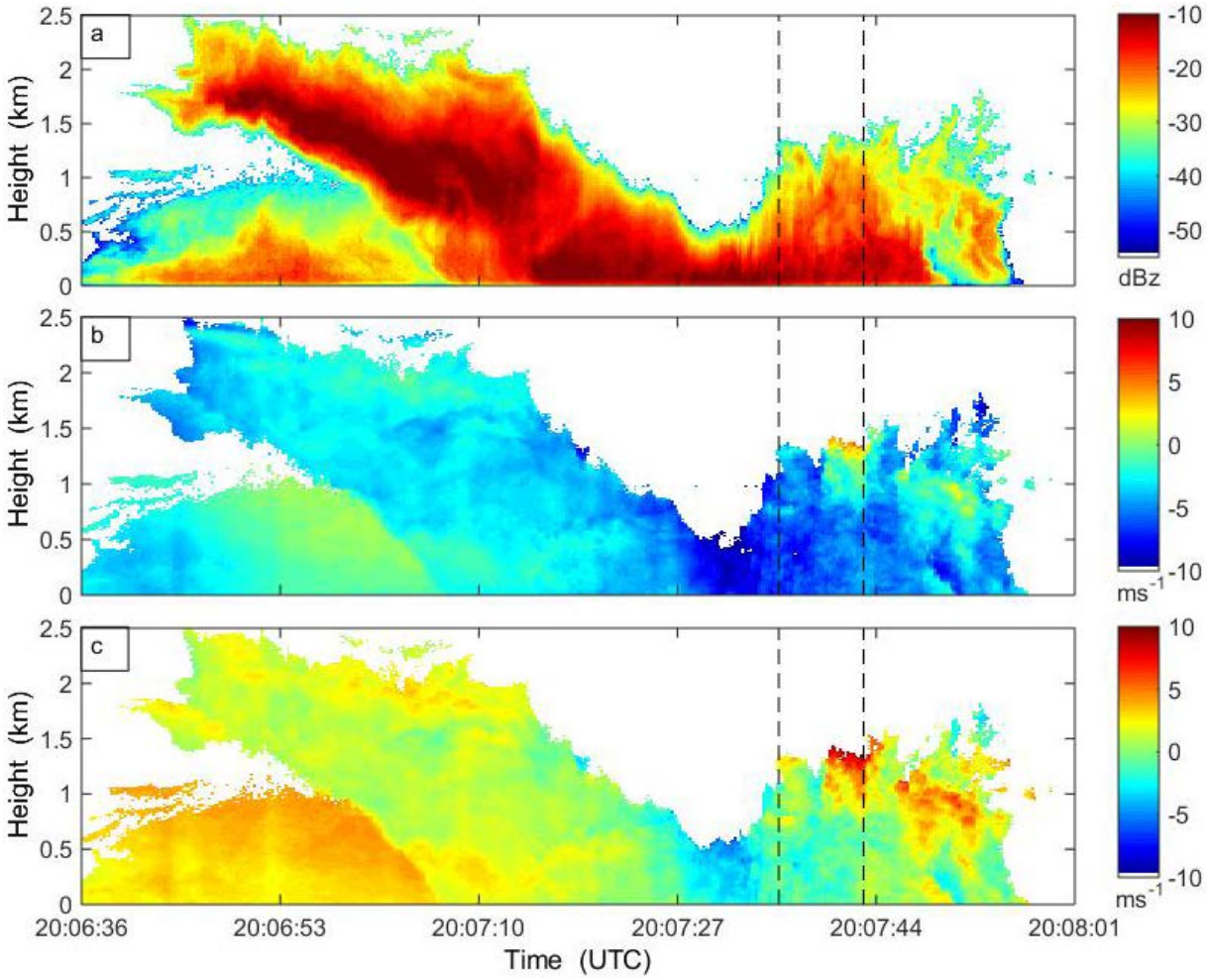

FIG. 2. Time-height cross section of (a) radar reflectivity, (b) aircraft motion corrected Doppler velocity (+: upward) and (c) aircraft motion uncorrected Doppler velocity in the precipitating cloud on 22 May 2012 during Key West experiment from 20:06:20 to 20:08:00 UTC. The reported height is above the Airborne Radar Level. Zero height corresponds to 450 m above sea level. Dashed lines indicates a specific time for the Doppler spectra in Fig. 4 and Fig. 5.

at cloud base level. However, downward motions before about 20:06:50 and upward motion after that in first cell may imply the possibility of some re-circulation within the cell that may help the growth of larger droplets. But, interpretation of the mean Doppler velocities is not straightforward due to the presence of embedded vertical air motion in the presence of precipitation.

4. Air-density-corrected terminal velocity

To retrieve vertical air velocity using Mie technique, an analytical relationship is required to transform Mie resonance from drop size domain to terminal velocity domain. This relationship is the Beard (1985) fit to the well-known Gunn and Kinzer (1949; hereafter GK49) terminal velocity data:

$$V_0(cm/s) = \exp(5.984 + 0.8515x - 0.1554x^2 - 0.03274x^3), \quad (1a)$$

where V_0 is the terminal velocity of a drop with diameter D in still air at sea surface and x = ln[D(mm)]. Since the GK49 measurements were made at sea level for still air conditions, a density correction is applied to the terminal velocity for the observations made aloft (at altitude z) by using the Beard (1985) formulation,

$$V_f = V_z = \left(\frac{\rho_0}{\rho_z}\right)^m V_o \quad (1b)$$

where ρ_o = 1.194 kg m^{-3} is the air density at z = 0 for standard conditions. The coefficient m is a function of the raindrop diameter of interest: m = 0.375 + 0.025 D [mm]. Hereafter, we will call the V_f as a density corrected fall velocity. V_f in Eq. (1b) is V_{f1} (will be seen later) when V_o of D_{1M} = 1.69 mm is used, where D_{1M} is the location of the first Mie minimum in terms of particle size. The ρ_z is the air density at altitude z and it can be written using Ideal Gas Law as

$$\rho_z = \frac{P}{R_d T_v} \quad (2a)$$

$$T_v = (1 + 0.608q)T \quad (2b)$$

where P is pressure, R_d the gas constant for dry air, T_v the virtual temperature, q the specific humidity and T the potential temperature at z. Fig. 3a shows the simulated Mie spectra in still air at different heights where P, q and T are retrieved from a sounding obtained between 19:24:00 and 19:39:00 UTC on 22 May 2012 in Key West, Florida. The blue curve is the spectrum at ground without air density correction whereas green and red curves are spectra at about 450 m and 1500 m above ground respectively. It can be seen that the spectra shift to the right with the increase of height, which reflects a gradually reduced air density leading to increased terminal speeds. Fig. 3b shows the air-density-corrected terminal speed profile above aircraft for the raindrop of 1.69 mm diameter. It is not a constant, but monotonically increases upward. This curve is used to find out the V_{f1} at different heights and the V_{f1} is in turn used to retrieve vertical air velocity at those heights.

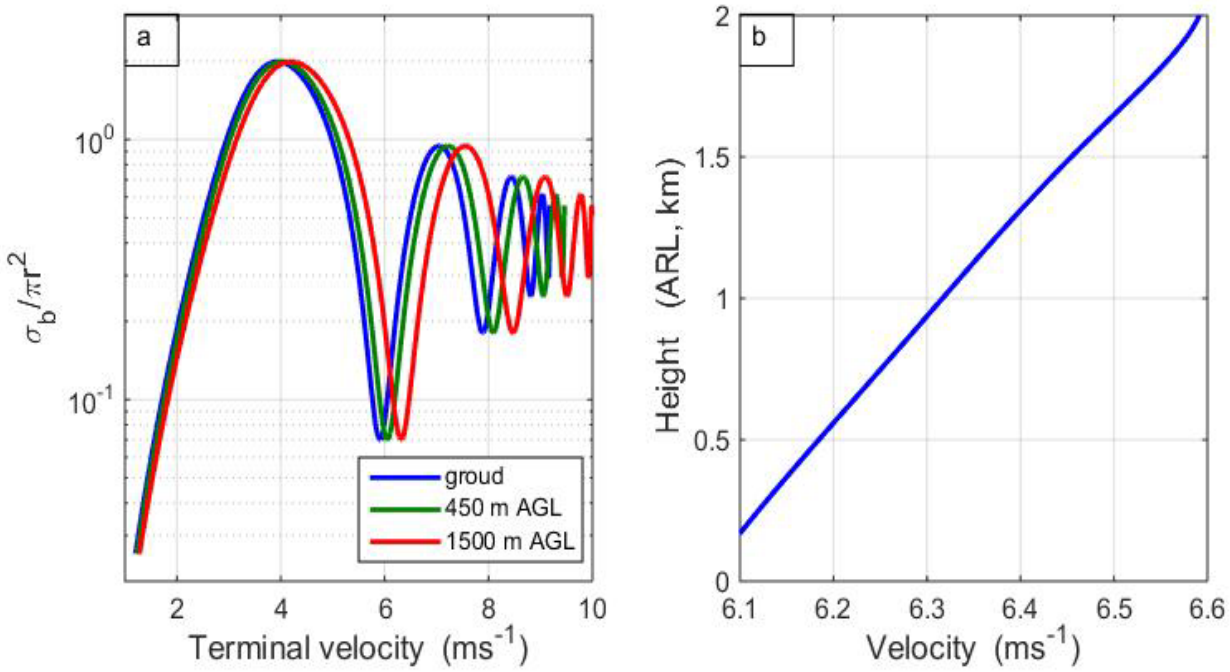

Fig. 3. Simulated Mie spectrum without air-density correction at ground, and spectra with air-density-corrected at 450 m and 1500 m above ground for observations obtained on 22 May 2012 in Barbados (b); air-density-corrected terminal speed, or V_{f1} profile above aircraft for the raindrop of 1.69 mm diameter.

5. Observed turbulent vertical air velocity

Vertical air velocity at a given range gate can be obtained through four steps. The first step involves removing contaminations from aircraft motion and horizontal wind. The second step establishes the first Mie minimum and its associated velocity. The third step uses the mothed introduced in section 4 to correct the velocity found in step 2 to the height of the range gate. The fourth step provides the difference between the velocity found in step 3 and its theoretical value at the same height. Applying these steps to all the range gates, one can obtain the vertical air velocity profile in a cloud layer when the Mie minimum is observed. Fig. 4 shows a case observed in Key West of Florida on 22 May 2012 at 20:07:42 UTC that is indicated by the right vertical dashed line in Fig. 2. What is shown in Fig. 4a is the Doppler spectrogram. Fig .4b is similar to Fig. 4a, but the aircraft motion and wind impact have been corrected. Compared with Fig .4a, the Doppler

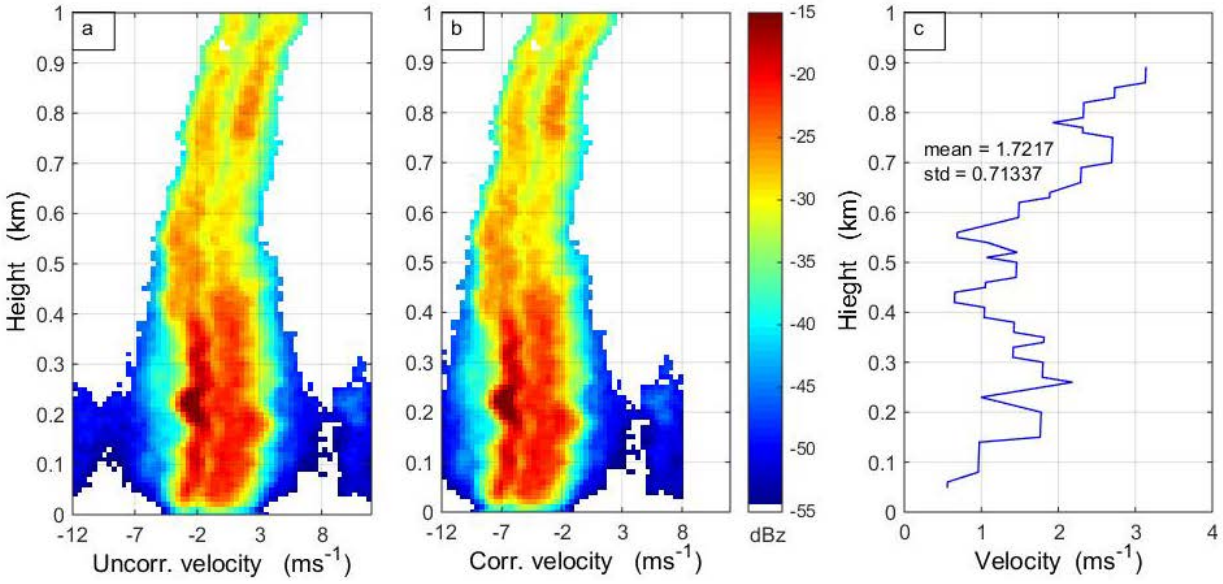

Fig. 4. Uncorrected Doppler spectrogram (a), corrected Doppler spectrogram (b), and retrieved vertical air velocity using Mie technique (c). They were obtained at 20:07:42 UTC on 22 May 2012 in Key West, Florida.

spectrogram has been shifted about 6 ms^{-1} to the left in Fig .4b. The vertical air velocity profile in Fig. 4c is obtained through the aforementioned 4-step procedure. Just as that shown in Fig. 4a and 4b for Doppler spectrograms, in Fig. 4c, the vertical range resolution is 10 m and the velocity resolution is 0.37 ms^{-1}. The mean value of the vertical air velocity in entire cloud layer is about 1.72 ms^{-1}, where the positive (negative) velocity indicates an upward (downward) air motion. The vertical air velocity is not spatially uniform and exhibits changes. For this case, turbulence or high frequency oscillations superposes on a velocity increasing with height. The standard deviation of the velocity in cloud layer is about 0.71 ms^{-1}. These turbulent motions or high frequency oscillations can also been seen from the saw-tooth-like echoes shown in the Doppler spectrograms in Fig. 4a and 4b. More specifically, if neglecting oscillations with one velocity resolution, one can find five layers in which the velocity increases with height and four layers in which the velocity decreases with height. Local convergence exists in the layers where velocity decreases and may enhance the collision-coalescence between hydrometers. This enhancement could repeat in each of the multiple layers where the velocity decreases and may help account for the relatively heavy precipitation falling out of these shallow clouds. Compared with velocity-decreasing layers, the velocity-increasing layers do not directly enhance the collision-coalescence between hydrometers, but they might be equally as important as the former layers because the increased vertical air velocities in these layers can carry size-increased or mass-increased cloud droplets to higher altitudes so that they can further increase in the velocity-decreasing convergent layers at higher levels.

Vertical air motion in a cloud layer is not necessarily always upward. Fig. 5 shows a case where the mean vertical air velocity is

about -0.09 ms^{-1}. It is observed in Key West of Florida on 22 May 2012 at 20:07:35 UTC that is indicated by the left vertical dashed line in Fig. 2. The negative mean velocity indicates a weak downward air motion. Turbulence or high frequency oscillations superposes on a nearly constant velocity with

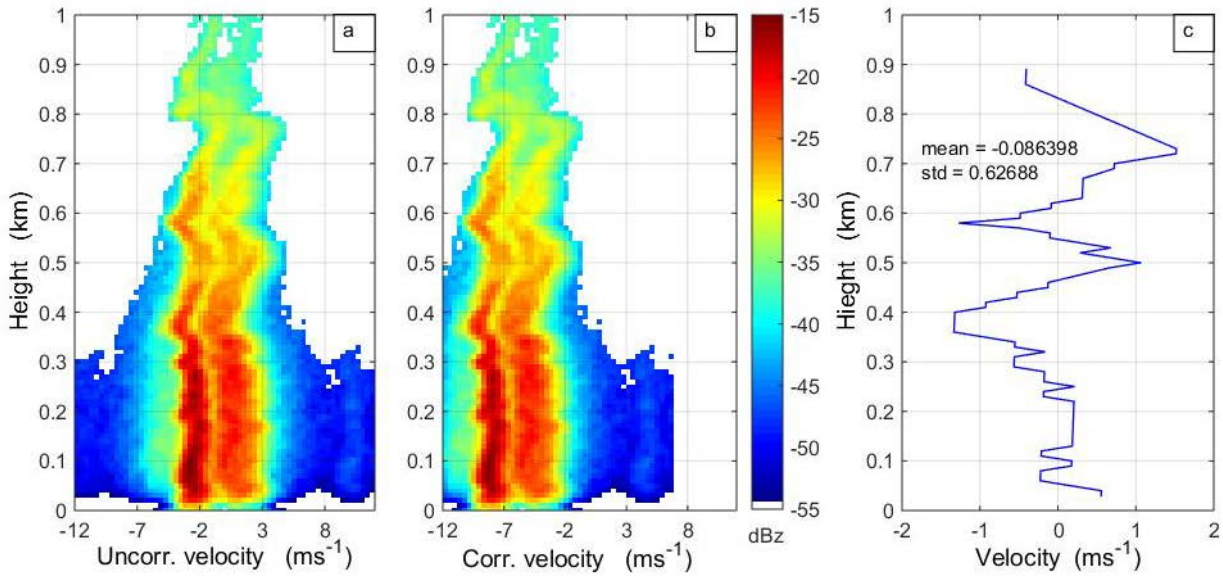

Fig. 5. Similar to Fig. 1 but obtained at 20:07:35 UTC on 22 May 2012 in Key West, Florida.

height. Again, these high frequency oscillations can also been seen from the saw-tooth-like echoes shown in Doppler spectrograms in Fig. 5a and 5b. Neglecting high frequency oscillations, the lowest velocity decreasing convergent layer is as deep as about 370 m. For this case, the standard deviation of vertical air velocity for the entire cloud layer is about 0.63 ms^{-1} and the largest magnitude of velocity variation between two consecutive turning points is about 2.8 ms^{-1}. Neglecting oscillations with one velocity resolution, there are two velocity increasing layers and five velocity decreasing layers. Similar to that occurring in the updraft case shown in Fig. 4, local convergence also occurs in the velocity decreasing layers in this downdraft case and could thus enhance the collision and coalescence process. Here, we neglect oscillations with one velocity

resolution because half a velocity resolution is less than the total uncertainty given in Appendix B.

In fact, turbulent vertical air velocity is not only observed in small cumulus during the field experiment conducted in Key West of Florida in 2012, but also observed during the field experiment conducted in Barbados in 2010 as shown in Fig. 6. Different from that in Fig. 4 and Fig. 5, the vertical air velocity profile in Fig. 6 is derived from the spectrum peaks of cloud returns that are observed on the right most in Fig. 6a and 6b. The Mie technique was not used because it can only retrieve the velocity below 0.6 km.

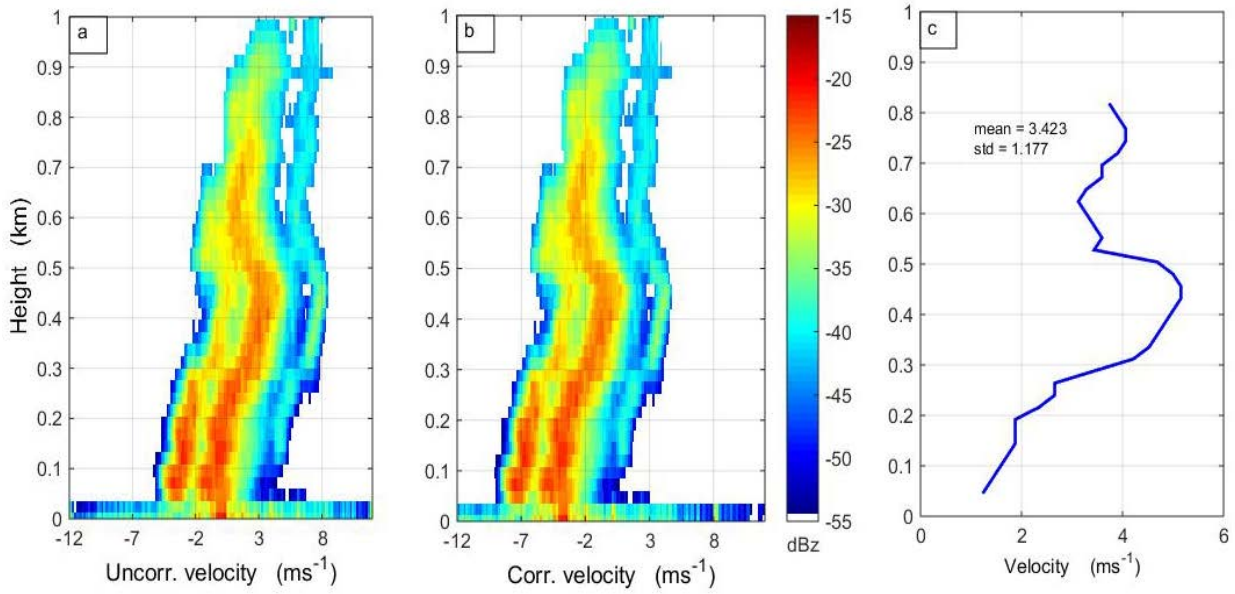

Fig. 6. Similar to Fig. 4 and Fig. 5, but observed at 16:17:52 UTC on 5 April 2010 in Barbados.

Observations presented in this section demonstrate that turbulent vertical air velocity and the associated enhancement of the collision-coalescence between hydrometers often exist in small cumulus clouds in both updraft and downdraft regions.

It is noteworthy that by using a one dimensional model and an updraft profile very similar to the one shown in Fig. 6c, Nelson (1971) investigated the warm rain initiation. He found an accumulation or generation zone where liquid water content

was higher just above the velocity maximum that coincides the velocity decreasing convergent layer discussed in this study. More specifically, Nelson showed that when coalescence equations were place in this generation zone this "… zone easily allows the coalescence process to produce rainfall in observationally reasonable times". Observations from airborne FMCW radar presented here strongly support the results obtained by Nelson from his model simulations. It has been realized for decades that turbulence may play a significant role in warm rain formation. This study show observational evidence for the first time that the collision-coalescence associated with turbulence or oscillations in the vertical air velocity may be an important process in the formation of warm rain precipitation.

6. Summary

Mie technique has been used for a decade to retrieve vertical air velocity in clouds from Doppler spectra observed by ground based cloud radar. This study applies the same technique to the data obtained by an airborne FMCW radar during the field experiment conducted in May 2012 in Key West of Florida. Equations proposed by previous investigators are adopted to correct the contributions from aircraft motion and horizontal wind to the Doppler velocity. It has shown that aircraft motion including both horizontal and vertical motion contributes most to the correction. Contribution from horizontal wind is comparable to that from aircraft motion whereas contribution from apparent motion, due to radar antenna not being located at the same location with INS unit, is negligible. After removing the contaminations from aircraft motion and horizontal wind, the shifted Doppler spectra are used to retrieve vertical air velocity in clouds. Neither updraft nor downdraft in cloud is spatially uniform. They exhibit

changes with height and turbulence or oscillations of vertical air velocity are observed. More specifically, there are multiple layers in which vertical air velocity increases or decreases with height. Local convergence exists in velocity decreasing layers and it enhances collision-coalescence between hydrometers. The velocity increasing layers embedded in updraft are able to carry not only small but also size-increased or mass-increased cloud droplets upward so that those cloud droplets can further increase in convergent layers at higher levels. These processes could repeat in each of the multiple layers and may help account for the relatively heavy precipitation falling out of these shallow clouds. It has been realized for decades that turbulence may play a significant role in warm rain formation. This study, for the first time, shows observational evidence that the collision-coalescence associated with turbulence or oscillations in the vertical air velocity may be an important process in the formation of warm rain precipitation.

Appendix A. Formulas for removal of contamination of motion

L1994 employed an angle between radar beam and XOZ plane, e.g. τ in their Fig. 3 that allows a convenient determination of a sampling volume location and the direction of position vector for their scanning beam. For our case, the radar beam is fixed and located in plane YOZ. Thus, angle τ is not needed and azimuth is equal to zero or $\lambda = 0$ (refer to Fig. 3 of L1994). The aircraft-relative Cartesian components of a position vector, x_a, y_a and z_a or Eq. (4) of L1994 can be rewritten as

$$\begin{pmatrix} x_a \\ y_a \\ z_z \end{pmatrix} = r \begin{pmatrix} 0 \\ \cos\phi \\ \sin\phi \end{pmatrix} \qquad \text{(A1)}$$

where r is the slant range from radar to a investigated radar resolution volume and ϕ is the elevation angle. In earth-relative

coordinate system, the Cartesian components of the vector are

$$\begin{pmatrix} x \\ y \\ z \end{pmatrix} = M_T M_D M_P M_R \begin{pmatrix} x_a \\ y_a \\ z_a \end{pmatrix} \qquad \text{(A2)}$$

where M_T, M_D, M_P, M_R are transformation matrices given by L1994. Substituting the expressions of M_T, M_D, M_P, and M_R into the above equation, one has

$$\begin{pmatrix} x \\ y \\ z \end{pmatrix} = r \begin{pmatrix} \cos H \sin R \sin\phi + \sin H \cos P \cos\phi - \sin H \sin P \cos R \sin\phi \\ \cos H \cos P \cos\phi - \sin H \sin R \sin\phi - \cos H \sin P \cos R \sin\phi \\ \sin P \cos\phi + \cos P \cos R \sin\phi \end{pmatrix} \qquad \text{(A3)}$$

where H is the heading of the aircraft, R the roll angle and P the pitch angle. Using Eq. 4 and Eq. 19 of L1994 and going through a series of mathematical manipulations similar to those given by L1994, one can obtain an analytical expression for radar measured Doppler velocity that is similar to the Eq. 26 of L1994. However, we are not interested in the Doppler velocity here. What we are interested in is the vertical air velocity. With a little further mathematical manipulation, one can easily obtain following analytical expressions

$$\left(\overline{w} - \overline{v}_t = \frac{V_r - I_1 + I_2 - I_3 - I_4}{\sin\phi} + WG \right) \qquad \text{(A4a)}$$

$$I_1 = \frac{ux + vy}{r} \qquad \text{(A4b)}$$

$$I_2 = \frac{VG\left(x \sin T + y \cos T\right)}{r} \qquad \text{(A4c)}$$

$$I_3 = -\frac{Lx}{r}\left[\left(1 + \cos P\right)\cos H \frac{dH}{dt} - \sin P \sin H \frac{dP}{dt}\right] \qquad \text{(A4d)}$$

$$I_4 = -\frac{L}{r}\left\{ z \cos P \frac{dP}{dt} - y\left[\left(1 + \cos P\right)\sin H \frac{dH}{dt} + \sin P \cos H \frac{dP}{dt}\right]\right\} \qquad \text{(A4e)}$$

where V_r is the radar measured radial velocity, *WG* the vertical velocity of the aircraft relative to the ground, *u* the component of horizontal wind in east direction, *v* the component of horizontal wind in north direction, *VG* the horizontal velocity of the aircraft relative to the ground. *L* is the distance between radar antenna and GPS navigation unit and it is about 1 m for our case. Compared with Eq. 26 of L1994, I_3 and I_4 have reversed signs because radar antenna in this study is mounted at the head of the aircraft whereas the antenna in L1994 was located at the tail of the aircraft. By using Eq. 4, aircraft motion and impact from horizontal wind as well as apparent motion due to the radar antenna being located some distance away from the navigation unit, can been removed.

Appendix B. Uncertainties

In previous discussions, we neglect changes with the magnitude of one velocity resolution because half of velocity resolution is less than the expected uncertainty resulting from the removal of aircraft motion and positioning first Mie minimum. Heymsfield (1989) discussed and formulated the bias and uncertainty in airborne Doppler radar measured radial velocity. The radial velocity uncertainties is related to the uncertainties in aircraft horizontal and vertical velocities as well as the aircraft attitude angles. For this study, the uncertainty of aircraft attitude angles is less than 0.1^o and the uncertainty of aircraft horizontal velocity is 5 ms^{-1} (Kalogiros and Wang, 2002). They are same as those numbers given by Heymsfield (1989) in his study, but CIRPAS has an approximate 60 ms^{-1} speed relative to ground in still air, which is only half of the value given by Heymsfield (1989). Thus, the uncertainty related to aircraft horizontal motion in this study should be ± 0.06 ms^{-1} or half of that given by Heymsfield (1989). The uncertainty

related to aircraft vertical motion is equal to the uncertainty of the aircraft vertical velocity itself, which is 0.05 ms^{-1} for CIRPAS (Kalogiros and Wang, 2002). Thus, the total uncertainty related to aircraft motion removal is ±0.11 ms^{-1}, the sum of the above two uncertainties. In fact, by using a high accuracy global navigation satellite systems aided inertial geopositioning system, Haimov and Rodi (2013) defined the aircraft motion correction for radar measured radial velocity as a radar pointing angle calibration problem. The root-mean-square error of the radar beam pointing angle they obtained is less than 0.03^{o} and the associated velocity error is less than 0.05 ms^{-1}. Calibrating antenna pointing angle is beyond the scope of this study, and considering the even higher precision in the measurements of aircraft height, velocity and altitude angles in the study of Haimov and Rodi (2013), we use ±0.11 ms^{-1} as a conservative estimate of the uncertainty for this study. By means of simulation, Lhermitte (2002) found a 0.066 ms^{-1} standard deviation in positioning the first Mie minimum location from a three order polynomial fitted Doppler spectrum. This study determines the first Mie minimum locations from the Doppler spectra that have been smoothed using a three order Savitzky-Golay filter, but velocities are still discrete with the resolution of 0.3937 ms^{-1} and the positioning uncertainty should be equal to the quantization uncertainty that can be calculated as $\sqrt{0.3937^2/12} \approx 0.1137\ ms^{-1}$ (Oliver etc., 1948). The total uncertainty is about 0.22 ms^{-1}.

In addition, for two selected instants shown in Fig. 4 and 5, our consideration is that the first Mie minimum must be clear and velocity can be retrieved unambiguously. The upward motion is located around the center and the downward motion is located around the edge of the third cell (refer to Fig. 2), which implies the possibility of some re-circulation within the cloud that may help the growth of larger droplets too.

Acknowledgement: This work was supported by ONR Grant N000140810465.

REFERENCES

Doviak, R. J., and D. S. Zrnić, 1993: *Doppler Radar and Weather Observations*. 2nd ed. Academic Press, 562 pp.

French, J. R., G. Vali, and R. D. Kelly, 1999: Evolution of small cumulus clouds in Florida: Observations of pulsating growth. *Atmos. Res.*, **52**, 143-165.

Giangrande, S. E., E. P. Luke, and P. Kollias, 2010: Automated Retrievals of Precipitation Parameters Using Non-Rayleigh Scattering at 95 GHz. *J. Atmos. Oceanic Technol.*, **27**, 1490-1503.

Gossard, E. E., 1988: Measuring drop-size distributions in clouds with a clear-air-sensing Doppler radar. *J. Atmos. Oceanic Technol.*, **5**, 640-649.

Gregory Falkovich, Mikhail G. Stepanov, and Marija Vucelja, 2006: Rain Initiation Time in Turbulent Warm Clouds. *J. Appl. Meteor. Climatol.*, **45**, 591–599. doi: http://dx.doi.org/10.1175/JAM2364.1

Haimov, S. and A. Rodi, 2013: Fixed-Antenna Pointing-Angle Calibration of Airborne Doppler Cloud Radar. *J. Atmos. Oceanic Technol.*, **30**, 2320–2335.

Heymsfield, G. M., 1989: Accuracy of vertical air motions from nadir-viewing Doppler airborne radars. *J. Atmos. Oceanic Technol.*, **6**, 1079-1082.

Heymsfield, G. M., and Coauthors, 1996: The EDOP radar system on the high-altitude NASA ER-2 aircraft. *J.*

Atmos. Oceanic Technol., **13**, 795-809.

Jennifer D. Small and Patrick Y. Chuang, 2008: New Observations of Precipitation Initiation in Warm Cumulus Clouds. *J. Atmos. Sci.*, **65**, 2972–2982. doi: http://dx.doi.org/10.1175/2008JAS2600.1

Lhermitte, R., 1988: Observation of rain at vertical incidence with a 94 GHz Doppler radar: An insight of Mie scattering. *Geophys. Res. Lett*., **15,** 1125-1128.

Kalogiros, J. A. and Q. Wang, 2002: Calibration of a Radome-Differential GPS System on a Twin Otter Research Aircraft for Turbulence Measurements. *J. Atmos. Oceanic Technol.*, **19**, 159–171.

Kollias, P., B. A. Albrecht, and F. Marks Jr., 2002: Why Mie? Accurate observations of vertical air velocities and raindrops using a cloud radar. *Bull. Amer. Meteor. Soc*., **83**, 1471–1483.

Kollias, P., B. A. Albrecht, and F. Marks Jr., 2003: Cloud radar observations of vertical drafts and microphysics in convective rain. *J. Geophys. Res*., **108**, 4053, doi: 10.1029/2001JD002033.

Lau, K.-M., and H.-T. Wu, 2003: Warm rain processes over tropical oceans and climate implications. Geophys. Res. Lett., 30, 2290, doi: 10.1029/2003GL018567.

Lee, W.-C., P. Dodge, F. Marks, and P. Hildebrand, 1994: Mapping of airborne Doppler radar data. *J. Atmos. Oceanic Technol*., **11**, 572–578.

Lhermitte, R., 1988: Observation of rain at vertical incidence with a 94 GHz Doppler radar: An insight of Mie scattering. *Geophys. Res. Lett*., **15,** 1125-1128.

May, P. T., and D. K. Rajopadhyaya, 1996: Wind profiler observations of vertical motion and precipitation microphysics of a tropical squall line. *Mon. Wea. Rev.*, **124**, 621–633.

Nelson, L. D., 1971: A Numerical Study on the Initiation of Warm Rain. *J. Atmos. Sci.*, **28**,752–762. doi: http://dx.doi.org/10.1175/1520-0469(1971)028<0752:ANSOTI>2.0.CO;2

Oliver, B. M., J. R. Pierce, and C. E. Shannon, 1948: "The Philosophy of PCM", *Proceedings of the IRE*, Vol. **36**, pp. 1324–1331.

Probert-Jones, J. R. and W. G. Harper, 1961: Vertical air motion in showers as revealed by Doppler radar. *Proc. Ninth Weather Radar Conf.,* Kansas City, MO, Amer. Meteor. Soc., 225-232.

Rajopadhyaya, D. K., P. T. May, R. Cifelli, S. K. Avery, C. R. Williams, W. L. Ecklund, and K. S. Gage, 1998: The effect of vertical air motions on rain rates and median volume diameter determined from combined UHF and VHF wind profiler measurements and comparisons with rain gauge measurements. *J. Atmos. Oceanic Technol*., **15**, 1306-1319.

Riemer and Wexler, 2005: Droplets to Drops by Turbulent Coagulation. *J. Atmos. Sci.*, **62**, 1962–1975. doi: http://dx.doi.org/10.1175/JAS3431.1

Saffman, P. G., and J. S. Turner, 1956: On the collision of drops in turbulent clouds. *J. Fluid Mech.*, **1,** 16–30.

Wakasugi, K., A. Mizutani, M. Matsuo, S. Fukao, and S. Kato, 1986: A direct method for deriving drop-size distribution and vertical air velocities

from VHF Doppler radar spectra. *J. Atmos. Oceanic Technol.,* **3**, 623–629.

Xue, Y, L. Wang, and W. W. Grabowski, 2008: Growth of Cloud Droplets by Turbulent Collision–Coalescence. *J. Atmos. Sci.*, **65**, 331–356.